

Nonlinear effects in buoyancy-driven variable density turbulence

P. Rao^{1†}, C. P. Caulfield^{2,3} & J. D. Gibbon⁴

¹Department of Applied Mathematics and Statistics, State University of New York, Stony Brook, NY 11790, USA

²BP Institute, University of Cambridge, Madingley Rise, Madingley Road, Cambridge CB3 0EZ, UK

³ Department of Applied Mathematics & Theoretical Physics, University of Cambridge, Centre for Mathematical Sciences, Wilberforce Road, Cambridge CB3 0WA, UK

⁴Department of Mathematics, Imperial College London, London SW7 2AZ, UK

We consider the time-dependence of a hierarchy of scaled L^{2m} -norms $D_{m,\omega}$ and $D_{m,\theta}$ of the vorticity $\boldsymbol{\omega} = \nabla \times \mathbf{u}$ and the density gradient $\nabla\theta$, where $\theta = \log(\rho^*/\rho_0^*)$, in a buoyancy-driven turbulent flow as simulated by Livescu & Ristorcelli (2007). $\rho^*(\mathbf{x}, t)$ is the composition density of a mixture of two incompressible miscible fluids with fluid densities $\rho_2^* > \rho_1^*$ and ρ_0^* is a reference normalisation density. Using data from the publicly available Johns Hopkins Turbulence Database, we present evidence that the L^2 -spatial average of the density gradient $\nabla\theta$ can reach extremely large values at intermediate times, even in flows with low Atwood number $At = (\rho_2^* - \rho_1^*)/(\rho_2^* + \rho_1^*) = 0.05$, implying that very strong mixing of the density field at small scales can arise in buoyancy-driven turbulence. This large growth raises the possibility that the density gradient $\nabla\theta$ might blow up in a finite time.

1. Introduction

The irreversible mixing at a molecular level of two fluids of different densities $\rho_2^* > \rho_1^*$ is a fluid dynamical process of great fundamental interest and practical importance, especially when the fluids are turbulent. Such turbulent mixing flows occur in many different circumstances. A particularly important class arises when the buoyancy force associated with the effects of statically unstable variations in fluid density in a gravitational field actually drives both the turbulence and the ensuing mixing itself. Such flows, commonly referred to as ‘Rayleigh-Taylor instability’ (RTI) flows due to the form of the initial linear instability (Rayleigh 1900; Taylor 1950), have been very widely studied (see Sharp (1984); Youngs (1984, 1989); Glimm *et al.* (2001); Dimonte *et al.* (2004); Dimotakis (2005); Lee *et al.* (2008); Hyunsun *et al.* (2008); Andrews & Dalziel (2010)), not least because of their relevance in astrophysics (Cabot & Cook 2006) and fusion (Petrasso 1994).

A key characteristic of RTI flows is that the developing turbulence is not driven by some external forcing mechanism, but rather is supplied with kinetic energy by the conversion of ‘available’ potential energy stored in the initial density field. This kinetic energy naturally drives turbulent disorder and a cascade to small scales, with an attendant increase in the dissipation rate of kinetic energy. Such small scales also lead to ‘filamentation’, i.e. enhanced surface area of contact between the two miscible fluids and, crucially, substantially enhanced gradients in the density field, which thus also leads to irreversible

† Email address for correspondence: prao@ams.sunysb.edu

mixing, and hence modification in the density distribution. There has been an explosion in interest in investigating the ‘efficiency’ of this mixing, i.e. loosely, the proportion of the converted available potential energy which leads to irreversible mixing, as opposed to viscous dissipation, (see the recent review of Tailleux (2013)), although the actual definition and calculation of the efficiency is subtle and must be performed with care – see for example Davies-Wykes & Dalziel (2014) for further discussion.

Nevertheless, there is accumulating evidence that buoyancy-driven turbulence is particularly efficient in driving mixing (Lawrie & Dalziel 2011; Davies-Wykes & Dalziel 2014) and certainly more efficient than externally forced turbulent flow. This evidence poses the further question whether there are distinguishing characteristics of the buoyancy-driven turbulent flow that are different from the flow associated with an external forcing, in particular whether these characteristics can be identified as being responsible for the enhanced and efficient mixing.

The situation is further complicated by the observation that, even when the two fluids undergoing mixing are themselves incompressible, since molecular mixing generically changes the specific volume of the mixture, the velocity fields of such ‘variable density’ (VD) flows, (following the nomenclature suggested by Livescu & Ristorcelli (2007)) are, in general, not divergence-free. This is certainly the case when the two densities are sufficiently different such that the Boussinesq approximation may not be applied. Commonly, the Boussinesq approximation is applied when the Atwood number At , defined as

$$At = \frac{\rho_2^* - \rho_1^*}{\rho_2^* + \rho_1^*}, \quad (1.1)$$

is small; i.e. $At \ll 1$. However, as discussed in detail in Livescu & Ristorcelli (2007), non-Boussinesq effects may occur when gradients in the density field become large. Following Cook & Dimotakis (2001) and Livescu & Ristorcelli (2007), the composition density $\rho^*(\mathbf{x}, t)$ of a mixture of two constant fluid densities ρ_1^* and ρ_2^* ($\rho_2^* > \rho_1^*$) is expressed in dimensionless form by

$$\frac{1}{\rho^*(\mathbf{x}, t)} = \frac{Y_1(\mathbf{x}, t)}{\rho_1^*} + \frac{Y_2(\mathbf{x}, t)}{\rho_2^*}, \quad (1.2)$$

where $Y_i(\mathbf{x}, t)$ ($i = 1, 2$) are the mass fractions of the two fluids and $Y_1 + Y_2 = 1$. (1.2) shows that the composition density ρ^* is bounded by $\rho_1^* \leq \rho^*(\mathbf{x}, t) \leq \rho_2^*$. Assuming that there is Fickian diffusion, the mass transport equations for the two species are

$$\partial_t(\rho Y_i) + \nabla \cdot (\rho^* Y_i \mathbf{u}) = Pe_0^{-1} \nabla \cdot (\rho \nabla Y_i), \quad (1.3)$$

where Pe_0 is the Péclet number: the dimensionless Reynolds, Schmidt and Péclet numbers are defined in table 1. Since the specific volume $1/\rho^*$ changes due to mixing, a non-zero divergence is induced in the velocity field which affects the conventional continuity equation for mass conservation

$$\partial_t \rho^* + \nabla \cdot (\rho^* \mathbf{u}) = 0, \quad (1.4)$$

which is derived from the sum over the two species in (1.3). In Appendix A, it is shown that the full equations for ρ^* derived from (1.2) and (1.3) take the form (see (A 6) and (A 7))

$$(\partial_t + \mathbf{u} \cdot \nabla) \rho^* = Pe_0^{-1} \rho^* \Delta(\ln \rho^*). \quad (1.5)$$

$$\nabla \cdot \mathbf{u} = -Pe_0^{-1} \Delta(\ln \rho^*). \quad (1.6)$$

As discussed in Livescu & Ristorcelli (2007), the Boussinesq approximation leads to the requirement that the velocity field is divergence-free $\nabla \cdot \mathbf{u} = 0$, in which case the mass

conservation equation becomes

$$\partial_t \rho^* + \mathbf{u} \cdot \nabla \rho^* = Pe_0^{-1} \Delta \rho^*. \quad (1.7)$$

This relies on the requirement that the second (nonlinear) term on the right hand side of (1.5) can be ignored compared to the first term, i.e. that

$$|\nabla \rho^*|^2 \ll \rho^* |\Delta \rho^*|. \quad (1.8)$$

As noted by Livescu & Ristorcelli (2007), this condition may be violated if substantial gradients develop in the density field. It is not *a priori* clear, even when the Atwood number is very small, that the non-divergence-free nature of the velocity field qualitatively changes the properties of the turbulent flow in ways which are significant to the mixing, and specifically whether regions in the flow may develop where the condition (1.8) is violated. This issue can be explored by careful numerical simulation, as reviewed by Livescu (2013), with a key observation (see Livescu & Ristorcelli (2007) for more details) being that the pressure distribution is substantially modified by non-Boussinesq effects. Furthermore, the central role played by intermittency and anisotropy, as discussed in Livescu & Ristorcelli (2008), suggests that it would be instructive to focus carefully on the time-dependent evolution of nonlinearity within such buoyancy-driven, variable density flows using the full equations (1.5) and (1.6) *without* the approximation (1.8).

Indeed, using a normalization density $\rho_0^* = \frac{1}{2}(\rho_1^* + \rho_2^*)$, an interesting observation is that with

$$\theta(\mathbf{x}, t) = \ln \rho \quad \rho = \frac{\rho^*}{\rho_0^*}, \quad (1.9)$$

(1.5) becomes a diffusion-like equation coupled to a \mathbf{u} -field whose divergence is linked to two derivatives in θ

$$(\partial_t + \mathbf{u} \cdot \nabla) \theta = Pe_0^{-1} \Delta \theta, \quad \text{with} \quad \nabla \cdot \mathbf{u} = -Pe_0^{-1} \Delta \theta. \quad (1.10)$$

While ρ^* itself is bounded above and below, the two gradients $\nabla \rho$ or $\nabla \theta$ are of much greater interest. Mathematically, understanding the properties of these gradients may reveal something about the regularity or otherwise of solutions of the governing equations. Conversely, physically, the magnitudes of these gradients are central to the rate of irreversible mixing within the flow.

Following Livescu & Ristorcelli (2007), there is another way of looking at the growth of these gradients. Consider the equation for θ and introduce a new velocity field $\mathbf{v} = \mathbf{u} + Pe_0^{-1} \nabla \theta$. The Hopf-Cole-like transformation $\theta = \ln \rho$ in (1.9) then leads to an exact cancellation of the nonlinear terms in (1.10) to give

$$(\partial_t + \mathbf{v} \cdot \nabla) \rho = Pe_0^{-1} \Delta \rho, \quad \text{with} \quad \nabla \cdot \mathbf{v} = 0. \quad (1.11)$$

This is the linear advection diffusion equation driven by a divergence-free velocity field. Note that $\boldsymbol{\omega} = \text{curl } \mathbf{u} = \text{curl } \mathbf{v}$. However, the fact that \mathbf{v} is actually an (explicit) function of $\nabla \theta$ makes (1.11) less simple than it first appears. Nevertheless, this equation provides a hint as to how we might look at the dynamics in a descriptive way. Consider a one-dimensional horizontal section through a rightward moving wave of ρ at a snapshot in time: in the frame of the advecting velocity \mathbf{u} the relevant component of \mathbf{v} is greater on the back face of any part of the wave (where $\nabla \rho > 0$) than on the front face (where $\nabla \rho < 0$). Thus in the advecting frame, (1.11) implies that not only is there the usual advection and diffusion but also a natural tendency for the back of a wave to catch up with the front, thus leading to a natural and inevitable steepening of $\nabla \rho$.

While our explanation of this steepening process is heuristic, it is consistent with experimental observations, and raises several questions. To explore these, we have undertaken

a re-analysis of a dataset of D. Livescu, arising from the simulation of a buoyancy-driven flow very similar to that reported in Livescu & Ristorcelli (2007), which is freely available at the Johns Hopkins Turbulence Database (JHTDB). Using this re-analysis, there are three central questions which we wish to explore as the primary aims of this paper.

(i) First, can the growth of gradients in the density field be bounded or controlled in any meaningful way? Such bounds could yield valuable insights into the structure and regularity of the density field and the uniform validity of the Boussinesq approximation for flows with $At \ll 1$, which may explain the ‘efficiency’ of mixing associated with buoyancy-driven turbulence?

(ii) Alternatively, if the growth of density gradients fails to saturate and instead accelerates by drawing on available kinetic energy, is it fast enough for a singularity to form in a finite time? The rapid growth observed by Luo & Hou (2014*a,b*) in the vorticity field of a symmetric incompressible Euler flow in a cylinder (with $\mathbf{u} \cdot \hat{\mathbf{n}} = 0$ on the boundary) provides strong evidence of a singularity in that system. It is possible that buoyancy-driven variable density turbulence is another example, despite the difference in boundary conditions and the presence of diffusion. However, it ought to be pointed out that neither the data nor the methods used here are sufficient to answer this question definitively.

(iii) Does the nonlinear ‘depletion’ (a concept we define below) in three-dimensional Navier-Stokes turbulence survive when it is coupled to the density field? In tandem with question (i), is there any nonlinear depletion in this density field?

The method of analysis used to address these questions is based on that used to analyze multiple data-sets generated from the incompressible three-dimensional Navier-Stokes equations (Donzis *et al.* (2013); Gibbon *et al.* (2014); Gibbon (2015)) on a cubical domain $[0, L]^3$. Here, we review this method for completeness. The method involves taking higher L^p -norms of the vorticity

$$\Omega_m = \left(L^{-3} \int_{\mathcal{V}} |\boldsymbol{\omega}|^{2m} dV \right)^{1/2m}, \quad \text{for } m \geq 1, \quad (1.12)$$

which are, in effect, higher moments of the enstrophy field, each having the dimensions of a frequency. Symmetry considerations in the three-dimensional Navier-Stokes equations suggest that the following scaling is appropriate ($\varpi_0 = \nu L^{-2}$)

$$D_m = (\varpi_0^{-1} \Omega_m)^{\alpha_m}, \quad \text{where } \alpha_m = \frac{2m}{4m-3}. \quad (1.13)$$

In most theoretical analyses it is impossible to avoid gradients of $\boldsymbol{\omega}$ in expressions for the higher moments Ω_m thus causing great difficulties with closure. It has been shown in Gibbon (2015) that the sequence of D_m can be connected with D_1 in the following way ($m \geq 2$)

$$D_m = C_m D_1^{A_{m,\lambda}}, \quad \text{and} \quad A_{m,\lambda} = \frac{\lambda_m(t)(m-1)+1}{4m-3}, \quad (1.14)$$

where the set of exponents $\{\lambda_m(t)\}$, subject to $1 \leq \lambda_m \leq 4$, are time-dependent, and the C_m a set of positive constants. One way of explaining the use of the relation in (1.14) is this: instead of using higher L^{2m} -norms in the sequence $\{D_1; D_m(t)\}$, one examines the sequence $\{D_1; \lambda_m(t); C_m\}$. Thus, the enstrophy D_1 is taken as the main variable and the exponents $\{\lambda_m(t)\}$ are then monitored numerically. Following how these exponents vary in time thus captures how the scaled moments D_m vary in time. The lower bound $\lambda_m \geq 1$ comes from the fact that $\Omega_1 \leq \Omega_m$ which can be shown to be equivalent to $D_1^{\alpha_m/2} \leq D_m$.

The case $\lambda_m = 1$ lies at the lower bound. At $\lambda_m = 4$, $A_m = 1$, and so $D_m = C_m D_1$ in (1.14). In this situation, it is apparent that the Navier-Stokes nonlinearity is fully saturated. Computations in Donzis *et al.* (2013) and Gibbon *et al.* (2014) have shown that the λ -parameter used there lies in the range $1.15 \leq \lambda \leq 1.5$. It is this that we refer to as ‘nonlinear depletion’, because the higher order, appropriately scaled moments D_m do not ‘saturate’ nonlinearly.

As shown in §3.1, in the buoyancy-driven flow considered here, it is possible to define not only equivalent higher L^p -norms of the vorticity Ω_m and hence D_m to those defined in (1.12) and (1.13), (which we relabel as $\Omega_{m,\lambda}$ and $D_{m,\omega}$ to make the dependence on vorticity explicit) but also equivalent norms of $\nabla\theta$, which we refer to as $\Omega_{m,\theta}$ and $D_{m,\theta}$. We can then investigate the equivalent nonlinear depletion in the density gradients through considering the rate of growth of $D_{1,\theta}$ and then monitoring the evolution of the exponents $\lambda_{m,\theta}(t)$ in the nonlinear growth terms, while also taking into account $D_{1,\omega}$. While it is not currently possible to answer definitively the question posed about blow-up of the density gradients at intermediate times, before diffusive mixing might be presumed to smooth out the density distribution, this paper is meant to set the scene as a way of analyzing and interpreting future computations.

The rest of the paper is organized as follows. In section 2, we describe in detail the properties of the simulation data set which we re-analyse, and we then present the results of this re-analysis in section 3. Finally, we draw our conclusions in section 4.

2. Description of the database

As noted in the introduction, we use the Johns Hopkins Turbulence Database (JHTDB) (Livescu *et al.* 2014), a publicly available direct numerical simulation (DNS) database, to explore nonlinear depletion in buoyancy-driven turbulence. We have used the homogeneous buoyancy driven turbulence dataset for our study. For more information, please see <http://turbulence.pha.jhu.edu/datasets.aspx>.

The equations used for this problem are the miscible two-fluid incompressible Navier-Stokes equations given by :

$$\partial_t \rho^* + (\rho^* u_j)_{,j} = 0 \quad (2.1)$$

$$\partial_t(\rho^* u_i) + (\rho^* u_i u_j)_{,j} = -p_{,i} + \tau_{ij,j} + \frac{1}{Fr^2} \rho^* g_i \quad (2.2)$$

$$u_{j,j} = -\frac{1}{Re_0 Sc} (\ln \rho^*)_{,jj} \quad (2.3)$$

$$\tau_{ij} = \rho^* Re_0^{-1} (u_{i,j} + u_{j,i} - \frac{2}{3} \delta_{ij} u_{k,k}) \quad (2.4)$$

$$(2.5)$$

where ρ^* is the non-dimensional density of the mixture.

The individual densities of the two components, ρ_1^* and ρ_2^* , are constant, but due to changes in mass fractions of each species, the density of the mixture can change (1.2). For this reason, the divergence of velocity is dependent on the density as seen in equation (2.3). The value of the Atwood number, At , that characterizes the density difference, is 0.05 and represents a small departure from the Boussinesq approximation. Some of the other important simulation parameters are displayed in table 1, where L_0 is the non-dimensionalization length, U_0 is the reference velocity scale, μ_0 is the dynamic viscosity and D is the mass diffusivity.

Reynolds number	$Re_0 = \rho_0^* L_0 U_0 / \mu_0$	12500
Froude number	$Fr = U_0 / \sqrt{gL_0}$	1
Schmidt number	$Sc = \mu_0 / D \rho_0^*$	1
Peclét number	$Pe_0 = Re_0 Sc$	12500
Atwood number	$At = (\rho_2^* - \rho_1^*) / (\rho_2^* + \rho_1^*)$	0.05
Domain		$2\pi \times 2\pi \times 2\pi$
Domain Length	L	2π
Non-dimensionalization Length	L_0	1

TABLE 1. Simulation parameters

In the simulation run by Livescu and colleagues, the fluids are initialized as random blobs with periodic boundaries in each direction and an initial diffusion layer at the interface. At sufficiently late time, the statistically homogeneous turbulent flow generated by such conditions resembles the interior of the mixing layer (away from the edge effects) of the Rayleigh-Taylor instability at the turbulent stage (see Livescu & Ristorcelli (2007) for further discussion).

The inhomogeneities in the transport terms are important only at the edge and thus, it is safe to assume that the homogeneous simulation data under consideration describes the core of a fully-developed mixing layer. Eventually, the turbulent behaviour dies out as the fluids become sufficiently mixed at the molecular level.

The variable-density version of the petascale CFDNS code (Livescu *et al.* 2009) was used with an ideal-gas equation of state to carry out the direct numerical simulation on 1024^3 grid points (for more information on a similar numerical study, refer to Livescu & Ristorcelli (2007)). The solution algorithm in the code is based on the pseudo-spectral method. The pressure is computed from the Poisson equation using the projection method. Time integration is achieved using the third order predictor-corrector Adams-Bashforth-Moulton method. The resultant high resolution data has been stored as a sequence of 1015 files, starting from $t = 0$ to $t = 40.56$, each representing time-step data for 32^3 spatial points.

The velocity gradients in the database are calculated as a post-processing step using a fourth order central finite differencing approximation. In general, for calculating the gradients or the state variables at a particular spatial location between the stored grid points, either a fourth order spatial interpolation (for gradients) or a sixth order Lagrangian interpolation (for state variables) is used. To get the temporal values other than those which are stored in the database, a piecewise cubic Hermite interpolation is employed. For more information on the specific dataset functions used for interpolation and calculation of the gradients, please refer to Appendix B.

3. Results

3.1. Definitions

It is clear from (1.2) that the composition density ρ^* is bounded by $\rho_1^* \leq \rho^* \leq \rho_2^*$. Moreover, in Appendix C it is also shown that every $\|\rho^*\|_{L^{2m}}$ is bounded above by its initial data provided the advecting \mathbf{u} -field is regular. However, our interest lies more in $\nabla \rho^*$, both mathematically through its analogy with the vorticity field ω , and physically through its central role in irreversible mixing, although it is difficult to work with this quantity alone. To circumvent this problem, the variable θ introduced in (1.9) and satisfying (1.10) is an easier variable with which to work. The idea is to consider both $\nabla \theta$ and

$\boldsymbol{\omega} = \text{curl } \mathbf{u}$ in the higher (unscaled) norms $L^{2m}(\mathcal{V})$, (analogously, but slightly differently to those defined in (1.12) and (1.13)) defined for $(1 \leq m < \infty)$ by

$$\Omega_{m,\theta} = \left(\int_{\mathcal{V}} |\nabla\theta|^{2m} dV \right)^{1/2m}, \quad (3.1)$$

$$\Omega_{m,\omega} = \left(\int_{\mathcal{V}} |\boldsymbol{\omega}|^{2m} dV \right)^{1/2m}, \quad (3.2)$$

where L_0 is the non-dimensionalization length in the the database which rescales the volume of integration here to be $\mathcal{V} = [0, L/L_0]^3$. The natural sequence of Hölder inequalities

$$\Omega_{m,\theta} \leq \left(\int_{\mathcal{V}} |\nabla\theta|^{2(m+1)} dV \right)^{\frac{1}{2(m+1)}} \left(\int_{\mathcal{V}} 1 dV \right)^{\frac{1}{2m(m+1)}} = \left(\frac{L}{L_0} \right)^{\frac{3}{2m(m+1)}} \Omega_{m+1,\theta}, \quad (3.3)$$

has a multiplicative factor which is only unity when $L = L_0$. Remembering the definition of α_m from (1.13),

$$\alpha_m = \frac{2m}{4m-3} \quad (3.4)$$

then the exponent on L/L_0 in (3.3) is related to α_m and α_{m+1} by

$$\frac{3}{2m(m+1)} = \frac{1}{\alpha_{m+1}} - \frac{1}{\alpha_m}. \quad (3.5)$$

In turn, this leads us to define a natural dimensionless length

$$\ell_m = (L/L_0)^{1/\alpha_m}, \quad (3.6)$$

which turns (3.3) into $\ell_m \Omega_{m,\theta} \leq \ell_{m+1} \Omega_{m+1,\theta}$. Use of these length scales allows us to investigate the relationship between the various moments of the density gradients in the most natural fashion, to allow us to determine whether they exhibit nonlinear depletion (or not). The aim is to assume there exists a solution of (1.10) in tandem with the vorticity field $\boldsymbol{\omega}$. Motivated by the depletion properties studied in Donzis *et al* (2013) and Gibbon *et al* (2014) for the Navier-Stokes equations, the following definitions are made

$$D_{m,\theta} = (\ell_m \Omega_{m,\theta})^{\alpha_m}; \quad D_{m,\omega} = (\ell_m \Omega_{m,\omega})^{\alpha_m}. \quad (3.7)$$

In the JHT-database the dimensionless domain size is 2π thus indicating that $L/L_0 = 2\pi$. The α_m -scaling in (3.7) has its origins in scaling properties of the three-dimensional Navier-Stokes equations (see Gibbon *et al.* (2014)). Then, as in (1.13) above, we consider

$$D_{m,\theta}(t) = D_{1,\theta}^{A_{m,\theta}(t)}, \quad (3.8)$$

where the multiplicative set of constants C_m have here been taken as unity. Following this, the JHT-database shows that the relation between $D_{m,\theta}$ and $D_{1,\theta}$ takes the form of (3.8). The data are consistent with $A_{m,\theta}(t)$ being expressed as

$$A_{m,\theta}(t) = \frac{\lambda_{m,\theta}(t)(m-1) + 1}{4m-3}, \quad 1 \leq \lambda_{m,\theta} \leq 4, \quad (3.9)$$

The $D_{m,\theta}(t)$ are thus defined in terms of the set $\{D_{1,\theta}(t), \lambda_{m,\theta}(t)\}$. There is also an equivalent formula for $D_{m,\omega}$ in terms of the set $\{D_{1,\omega}(t), \lambda_{m,\omega}(t)\}$. There is a lower bound $\lambda_{m,\theta} \geq 1$ for the same reasons given in the introduction for the equivalent quantities D_m and D_1 , as defined in (1.13). Numerically the $\lambda_{m,\theta}(t)$ can be calculated from the JHT-database by considering $\ln D_{m,\theta} / \ln D_{1,\theta}$. Note that the ordering observed

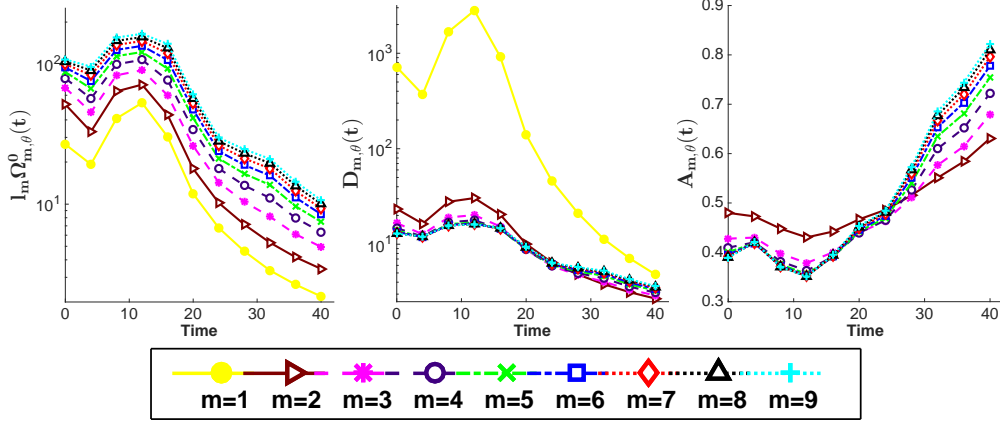


FIGURE 1. Time variation of: (a) $l_m \Omega_{m,\theta}(t)$, as defined in (3.2); (b) $D_{m,\theta}(t)$, as defined in (3.7); (c) $A_{m,\theta}(t)$ as defined in (3.8).

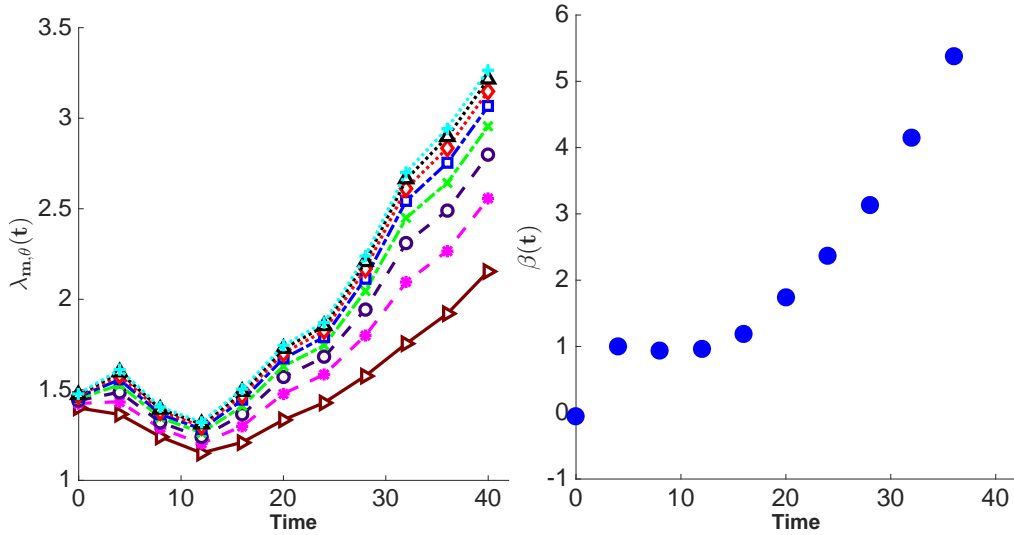


FIGURE 2. Time variation of: (a) $\lambda_{m,\theta}(t)$, as defined in (3.9), which fan out and grow with time; (b) $\beta(t)$ as defined in (3.12).

in (3.3) does not necessarily hold for the $D_{m,\theta}$ or the $D_{m,\omega}$ because α_m decreases with m .

3.2. The evolution of $D_{1,\theta}$

Formally consider the time evolution of $\int_{\mathcal{V}} |\nabla\theta|^2 dV$ using (1.10) and the relation for $\nabla \cdot \mathbf{u}$ in (1.10)

$$\begin{aligned} \frac{1}{2} \frac{d}{dt} \int_{\mathcal{V}} |\nabla\theta|^2 dV &= \int_{\mathcal{V}} \nabla\theta \cdot (Pe_0^{-1} \Delta - \nabla\mathbf{u}) \cdot \nabla\theta dV + \frac{1}{2} \int_{\mathcal{V}} |\nabla\theta|^2 (\nabla \cdot \mathbf{u}) dV \quad (3.10) \\ &\leq -Pe_0^{-1} \int_{\mathcal{V}} |\Delta\theta|^2 dV + \int_{\mathcal{V}} |\nabla\theta|^2 |\nabla\mathbf{u}| dV + \frac{1}{2} Pe_0^{-1} \int_{\mathcal{V}} |\nabla\theta|^2 |\Delta\theta| dV. \end{aligned}$$

Using the fact that $D_{1,\theta} = 2\pi \Omega_{1,\theta}^2$ together with the $D_{m,\theta} - D_{1,\theta}$ relation in (3.8) and

(3.9), Appendix D shows how this can be manipulated into the differential inequality

$$\frac{d}{dt}D_{1,\theta} \leq -\frac{D_{1,\theta}^2}{4\pi Pe_0 \|\theta\|_2^2} + 4\pi c_m Pe_0^{-1} D_{1,\theta}^{1+\lambda_{m,\theta}(t)} + 2\pi Pe_0 D_{1,\omega}, \quad (3.11)$$

where the $\lambda_{m,\theta}(t)$ appear in the exponent of the middle term on the right hand side. Plots of $\ell_m \Omega_{m,\theta}(t)$, $D_{m,\theta}(t)$ and $A_{m,\theta}$ are shown in figure 1, with plots of the corresponding $\lambda_{m,\theta}(t)$ in figure 2a: the relevant constants have not been estimated. Note that the set $\{\lambda_{m,\theta}(t)\}$ fan out with time with no tendency to coincide. Nonlinear depletion occurs when $A_{m,\theta} < 1$, which figure 1 shows is the case. Because $\lambda_{m,\theta}(t) \geq 1$, the exponent $1 + \lambda_{m,\theta}(t) \geq 2$. Given the values of $\lambda_{m,\theta}(t)$ in figure 2a, it is clear that despite the boundedness of $\|\theta\|_2^2$, the negative $D_{1,\theta}^2$ -term will always be smaller than the middle nonlinear term $Pe_0^{-1} D_{1,\theta}^{1+\lambda_{m,\theta}}$ for all non-small values of $D_{1,\theta}$.

There is also the issue of the size of the additive $2\pi Pe_0 D_{1,\omega}$ -term in (3.11). To turn this term into a term depending on $D_{1,\theta}$ alone requires a relation between $D_{1,\theta}$ and $D_{1,\omega}$, with the latter representing the fluid vorticity. Analytically, we have been unable to establish a relation between them but the JHT data-base provides us with a relation with a further exponent which we call $\beta(t)$

$$D_{1,\omega} = D_{1,\theta}^{\beta(t)}, \quad (3.12)$$

where the growth in the exponent $\beta(t)$ is shown in figure 2b. Figure 3 shows that the $Pe_0 D_{1,\theta}^{\beta(t)}$ -term (plotted with green squares) in (D 6) is dominant over the $Pe_0^{-1} D_{1,\theta}^{1+\lambda_{m,\theta}(t)}$ -term (plotted with red triangles), even when $\lambda_{m,\theta}(t)$ is chosen to be the maximum across m at each particular time step. The plots of $1 + \lambda_{m,\theta}$ and $\beta(t)$ both show that the values of these two quantities are both greater than two and thus cannot be controlled by the $-D_{1,\theta}^2$ term in (3.11). *The conclusion is that these estimates do not point to any mechanism of saturation and so the possibility of exponential growth in, or even blow-up of $D_{1,\theta}$ in a finite time, cannot be discounted.* It is important to stress that this is not inconsistent with the physical intuition that at late times, diffusion should smooth out all density gradients. This analysis only points to the possibility that at intermediate times it is possible that the density gradients may become extremely large. Furthermore, the ‘‘fanning out’’ of the $\lambda_{m,\theta}(t)$ for various m suggests a highly complex time-dependent fine structure in the density field, although figure 3 shows that this variation is not essential to our central conclusion concerning the time dependence of $D_{1,\theta}$.

Finally, figure 4 shows the equivalent set of plots of the time variation of $\ell_m \Omega_{m,\omega}(t)$, $D_{m,\omega}(t)$ and $A_{m,\omega}(t)$ defined as

$$A_{m,\omega}(t) = \ln D_{m,\omega} / \ln D_{1,\omega}. \quad (3.13)$$

In figure 5, we also show the time variation of the corresponding $\lambda_{m,\omega}(t)$, calculated using the analogous relationship

$$A_{m,\omega}(t) = \frac{\lambda_{m,\omega}(t)(m-1) + 1}{(4m-3)}. \quad (3.14)$$

It is apparent that the turbulent fluid part of the problem, which drives and dominates the system, has corresponding $\lambda_{m,\omega}(t)$ that are flat in time and sit in the range $1 < \lambda_{m,\omega} < 2$. This is consistent with the behaviour found in three-dimensional Navier-Stokes flow described in Donzis *et al* (2013), Gibbon *et al* (2014) and Gibbon (2015). Note that this contrasts strongly with the behaviour of the θ -variable where the $\lambda_{m,\theta}$ fan out and grow in time, as shown in figure 2, and suggests, in some as yet unexplored

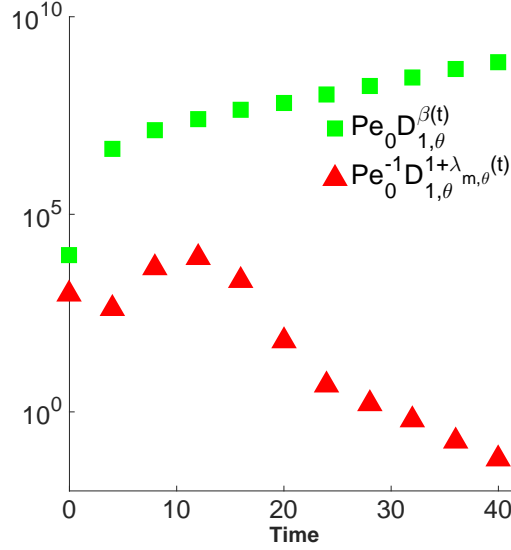


FIGURE 3. Time variation of $Pe_0 D_{1,\theta}^{\beta(t)}$ (plotted with green squares) and $Pe_0^{-1} D_{1,\theta}^{1+\lambda_{m,\theta}(t)}$ -term (plotted with red triangles) where $\lambda_{m,\theta}(t)$ is chosen to be the maximum value over m at each time step with $Pe_0 = 12,500$.

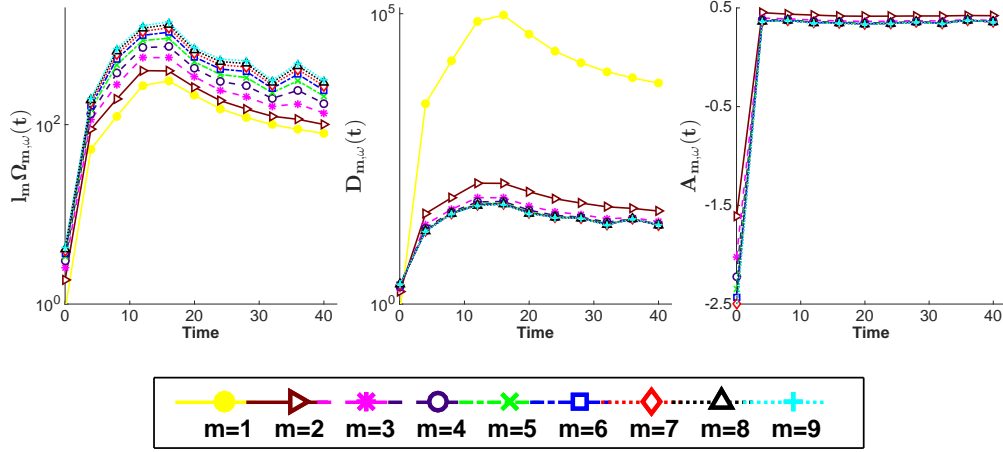
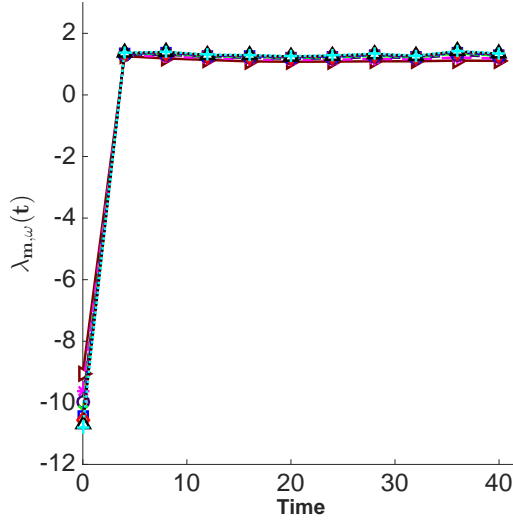


FIGURE 4. Time variation of: (a) $l_m \Omega_{m,\omega}(t)$ as defined in (3.2); (b) $D_{m,\omega}(t)$, defined in (3.7); (c) $A_{m,\omega}(t)$, as defined in (3.14).

sense, that the density gradient field is even more complex than the vorticity field in this buoyancy-driven flow, in particular that the nonlinear depletion is appreciably weaker in the density gradient field.

4. Conclusions

We have studied the growth of $D_{1,\theta} = 2\pi \int_V |\nabla\theta|^2 dV$ (and $D_{1,\omega} = 2\pi \int_V |\omega|^2 dV$) based on the evolution of $\nabla\theta$ with $\theta = \ln(\rho^*/\rho_0^*)$ as expressed in equation (1.10). The differential inequality for $D_{1,\theta}$ shown in (3.11) contains the set of exponents $\lambda_{m,\theta}$ ($m = 2, \dots, 8$) together with $\beta(t)$, which is the exponent that connects $D_{1,\theta}$ with $D_{1,\omega}$. These have been calculated directly from the JHTDB-database data which has been employed in

FIGURE 5. Time variation of $\lambda_{m,\omega}(t)$, calculated using the relation (3.14).

this paper. The fan-like shape of the set $\lambda_{m,\theta}$ ($m = 2, \dots, 8$) and its growth in time is shown in figure 2a while the growth of β is shown in figure 2b.

The extraction of statistics for the higher moments D_m for $m \geq 2$ raises a similar question to that addressed in Donzis *et al* (2013) for the three-dimensional Navier-Stokes equations which was based on four data-sets. In three of them (a 2048×1024^2 and two 512^3 calculations) statistics were able to be reliably extracted for up to $m = 9$ but not beyond. In the 4096^3 calculation reliable extraction only up to $m = 6$ was achievable. Likewise, only reliable extraction up to $m = 9$ was achievable from the JHTDB-database. In the three-dimensional Navier-Stokes calculations a strong degree of convergence was observed for $m \geq 4$ suggesting, but not proving, that this set might ultimately converge to a finite D_∞ . Given the fan-like separation of the $\lambda_{m,\theta}$ in Fig. 2 it is not clear one way or the other whether convergence ultimately occurs to a finite D_∞ .

In tandem with the numerical evidence in figure 2a consistent with strong growth in $\nabla \rho^*$, varying degrees of nonlinear depletion are also observed in the sense that $A_{m,\theta} < 1$, and $A_{m,\omega} < 1$ (as in figures 4c and 5). Depletion in $A_{m,\theta}$ reduces as the growth of $\lambda_{m,\theta}$ to the value 3.5 in the final stages attests. Indeed, note that $\lambda_{m,\theta} = 4$ would give a linear relation and be equivalent to a full estimate of the nonlinearity. Depletion in $D_{1,\omega}$ is quite severe, as shown in figures 4c and 5, which is consistent with the same effect observed in Navier-Stokes flows. Despite this, the cross-effect of the turbulent fluid flow driving the growth of $D_{1,\theta}$ through the exponent $\beta(t)$ swamps the term $D_{1,\theta}^{1+\lambda_{m,\theta}}$ in (3.11).

The fact that $1 + \lambda_{m,\theta} \geq 2$, with $\beta(t)$ growing rapidly up to a value of 6, leaves open the possibility that $D_{1,\theta}$ could blow up in a finite time. The rapid growth observed by Luo & Hou (2014a,b) in their computations of the symmetric Euler equations with a boundary, with a clear indication of the formation of a finite time singularity, suggests that the problem in this paper should be analyzed in this light, despite the differences in boundary conditions, the presence of diffusion and the limited grid-size. While the blow-up question cannot be directly answered with the available data, the growth is sufficiently strong that the mixing could be driven down to near molecular scales where the validity of the model fails. Interestingly, $\lambda_{m,\omega}$ simultaneously saturates as in figure 5 showing that the turbulent fluid component is not amplified by the density growth. This hints

that buoyancy-driven turbulence may well be more intense in some real physical and mathematical sense than constant-density turbulence, which may explain the observed extremely efficient mixing possible in such flows.

Acknowledgements

We acknowledge, with thanks, the staff of IPAM UCLA where this collaboration began in the Autumn of 2014 on the programme ‘‘Mathematics of Turbulence’’. We would also like to thank C. Doering and D. Livescu for useful discussions. Research activity of C.P.C. is supported by EPSRC Programme Grant EP/K034529/1 (‘‘Mathematical Underpinnings of Stratified Turbulence’’). All the numerical data used is from the Johns Hopkins Turbulence Database (JHTDB) Livescu *et al.* (2014), a publicly available direct numerical simulation (DNS) database. For more information, please see <http://turbulence.pha.jhu.edu/>. We also thank the referees for suggesting substantial improvements.

Appendix A. The equations for the composite density

Following Cook & Dimotakis (2001) and Livescu & Ristorcelli (2007) the composition density $\rho^*(\mathbf{x}, t)$ of a mixture of two constant fluid densities ρ_1^* and ρ_2^* ($\rho_2^* > \rho_1^*$) is expressed by (1.2) where $Y(\mathbf{x}, t) = Y_2$ is the mass fraction of the heavier fluid. It is important to stress that the two fluids are assumed to be incompressible, yet we do not make the Boussinesq approximation and so the difference between the two densities is allowed to take arbitrary values. Under the transport of a (dimensionless) velocity field $\mathbf{u}(\mathbf{x}, t)$, ρ^* obeys the equation of conservation of mass

$$\partial_t \rho^* + \nabla \cdot (\rho^* \mathbf{u}) = 0, \quad (\text{A } 1)$$

and the species transport equation

$$\partial_t (\rho^* Y) + \nabla \cdot (\rho^* Y \mathbf{u} + \mathbf{j}_F) = 0, \quad (\text{A } 2)$$

where the divergence of the flux \mathbf{j}_F represents Fickian diffusion, i.e.

$$\mathbf{j}_F = -Pe_0^{-1} \rho^* \nabla Y. \quad (\text{A } 3)$$

The Péclet number has been defined in table 1. Given that the solution of (1.2) shows that $\rho^* Y$ is linear in ρ^* such that

$$\rho^* Y = a \rho^* + b, \quad a = \frac{\rho_2^*}{\rho_2^* - \rho_1^*}, \quad b = -\frac{\rho_1^* \rho_2^*}{\rho_2^* - \rho_1^*}, \quad (\text{A } 4)$$

equation (A 2) simplifies to

$$b \nabla \cdot \mathbf{u} = Pe_0^{-1} \nabla \cdot (\rho^* \nabla Y). \quad (\text{A } 5)$$

Noting from (A 4) that $\rho^* \nabla Y = -b \nabla (\ln \rho^*)$ the coefficient b cancels to make (A 5) and (A 1) into:

$$\nabla \cdot \mathbf{u} = -Pe_0^{-1} \Delta (\ln \rho^*). \quad (\text{A } 6)$$

$$(\partial_t + \mathbf{u} \cdot \nabla) \rho^* = Pe_0^{-1} \rho^* \Delta (\ln \rho^*), \quad (\text{A } 7)$$

which are equations (1.5) and (1.6).

Function	Spatial Differentiation	Spatial Interpolation	Temporal Interpolation
GetDensity()	FD4_DIFF_LAG4_INT	LAG6_INT	PCHIP_INT
GetDensityGradient()	FD4_DIFF_LAG4_INT	FD4_DIFF_LAG4_INT	PCHIP_INT
GetVelocityGradient()	FD4_DIFF_LAG4_INT	FD4_DIFF_LAG4_INT	PCHIP_INT

TABLE 2. Function names in the database corresponding to the interpolation of various quantities used for data analysis in the paper.

Appendix B. Details of Database

We have used the matlab analysis tools provided at the webpage http://turbulence.pha.jhu.edu/matlabanalysis_tools.aspx, to fetch the data from the database. For details regarding the computational domain, boundary conditions, numerical method, etc., please refer to <http://turbulence.pha.jhu.edu/docs/README-HBDT.pdf>.

Appendix C. Every $\|\rho^*\|_{L^{2m}(\mathcal{V})}$ decays in time

To prove the boundedness of each $\|\rho^*\|_{L^{2m}(\mathcal{V})}$ under a sufficiently regular advecting field \mathbf{u} we write

$$\frac{1}{2m} \frac{d}{dt} \int_{\mathcal{V}} |\rho^*|^{2m} dV = - \int_{\mathcal{V}} \rho^{*(2m-1)} \nabla \cdot (\rho^* \mathbf{u}) dV, \quad (\text{C1})$$

and

$$\rho^{*(2m-1)} \nabla \cdot (\rho^* \mathbf{u}) = \left(1 - \frac{1}{2m}\right) \rho^{*2m} \nabla \cdot \mathbf{u} + \frac{1}{2m} \nabla \cdot (\rho^{*2m} \mathbf{u}). \quad (\text{C2})$$

(C1) then becomes

$$\frac{1}{2m} \frac{d}{dt} \int_{\mathcal{V}} |\rho^*|^{2m} dV = - \left(1 - \frac{1}{2m}\right) \int_{\mathcal{V}} \rho^{*2m} \nabla \cdot \mathbf{u} dV \quad (\text{C3})$$

where the volume integral of the second term in (C2) is zero through the divergence theorem. Using (2.3), (C3), becomes

$$\begin{aligned} \frac{1}{2m} \frac{d}{dt} \int_{\mathcal{V}} |\rho^*|^{2m} dV &= Pe_0^{-1} \left(1 - \frac{1}{2m}\right) \int_{\mathcal{V}} \rho^{*2m} \Delta(\ln \rho^*) dV \\ &= -Pe_0^{-1} (2m-1) \int_{\mathcal{V}} \rho^{*2(m-1)} |\nabla \rho^*|^2 dV \\ &= -Pe_0^{-1} \frac{(2m-1)}{m^2} \int_{\mathcal{V}} |\nabla \rho^{*m}|^2 dV \leq 0. \end{aligned} \quad (\text{C4})$$

Thus, every L^{2m} -norm decays in time. ■

Appendix D. The differential inequality for $D_{1,\theta}$

Let us repeat (3.10) and proceed from there:

$$\frac{1}{2} \frac{d}{dt} \int_{\mathcal{V}} |\nabla \theta|^2 dV \leq -Pe_0^{-1} \int_{\mathcal{V}} |\Delta \theta|^2 dV + \int_{\mathcal{V}} |\nabla \theta|^2 |\nabla \mathbf{u}| dV + \frac{1}{2} Pe_0^{-1} \int_{\mathcal{V}} |\nabla \theta|^2 |\Delta \theta| dV. \quad (\text{D1})$$

Before going further it should be noted that a standard result connects $\nabla \mathbf{u}$, $\boldsymbol{\omega}$ and $\text{div } \mathbf{u}$

$$\begin{aligned} \int_{\mathcal{V}} |\nabla \mathbf{u}|^2 dV &= \int_{\mathcal{V}} |\boldsymbol{\omega}|^2 dV + \int_{\mathcal{V}} |\text{div } \mathbf{u}|^2 dV \\ &= \int_{\mathcal{V}} |\boldsymbol{\omega}|^2 dV + Pe_0^{-2} \int_{\mathcal{V}} |\Delta \theta|^2 dV \end{aligned} \quad (\text{D } 2)$$

For $m \geq 2$, and noting that $\frac{m-2}{2(m-1)} + \frac{m}{2(m-1)} = 1$, consider the term

$$\begin{aligned} \int_{\mathcal{V}} |\nabla \theta|^2 |\nabla \mathbf{u}| dV &\leq c_{1,m} \Omega_{1,\theta}^{\frac{m-2}{m-1}} \Omega_{m,\theta}^{\frac{m}{m-1}} [\Omega_{1,\omega} + Pe_0^{-1} \|\Delta \theta\|_2] \\ &\leq c_{2,m} D_{1,\theta}^{\frac{m-2}{2(m-1)}} D_{m,\theta}^{\frac{m}{\alpha_m(m-1)}} \left[(2\pi)^{-1/2} D_{1,\omega}^{1/2} + Pe_0^{-1} \|\Delta \theta\|_2 \right], \end{aligned} \quad (\text{D } 3)$$

where the factors of ℓ_m have been absorbed into the dimensionless constants $c_{1,m}$ and $c_{2,m}$. Now we turn to the idea introduced in §3.1 that connects $D_{m,\theta}$ with $D_{1,\theta}$ by using the formula (3.8) and (3.9) for $A_{m,\theta}$ and the set $\{\lambda_{m,\theta}(t)\}$. Inserting (3.8) into the right hand side of (D 3) gives (factors of 2π have also been absorbed into the constants)

$$\begin{aligned} \int_{\mathcal{V}} |\nabla \theta|^2 |\nabla \mathbf{u}| dV &\leq c_{2,m} D_{1,\theta}^{(1+\lambda_{m,\theta})/2} \left[(2\pi)^{-1/2} D_{1,\omega}^{1/2} + Pe_0^{-1} \|\Delta \theta\|_2 \right] \\ &\leq \frac{1}{2} Pe_0 D_{1,\omega} + c_{3,m} Pe_0^{-1} D_{1,\theta}^{1+\lambda_{m,\theta}} + \frac{1}{2} Pe_0^{-1} \|\Delta \theta\|_2^2, \end{aligned} \quad (\text{D } 4)$$

where the use of a Hölder inequality has split up the terms of the right hand side of (D 3). The same idea is used on the last term in (D 1) with $|\nabla \mathbf{u}|$ replaced by $|\Delta \theta|$:

$$\begin{aligned} Pe_0^{-1} \int_{\mathcal{V}} |\nabla \theta|^2 |\Delta \theta| dV &\leq (Pe_0^{-1} \|\Delta \theta\|_2^2)^{1/2} \left(c_{3,m} Pe_0^{-1} D_{1,\theta}^{1+\lambda_{m,\theta}} \right)^{1/2} \\ &\leq \frac{1}{2} Pe_0^{-1} \|\Delta \theta\|_2^2 + c_{4,m} Pe_0^{-1} D_{1,\theta}^{1+\lambda_{m,\theta}}. \end{aligned} \quad (\text{D } 5)$$

Altogether, (D 1) becomes

$$\frac{1}{4\pi} \dot{D}_{1,\theta} \leq -\frac{1}{4} Pe_0^{-1} \|\Delta \theta\|_2^2 + c_{5,m} Pe_0^{-1} D_{1,\theta}^{1+\lambda_{m,\theta}} + \frac{1}{2} Pe_0 D_{1,\omega}. \quad (\text{D } 6)$$

A simple integration by parts shows that

$$\|\nabla \theta\|_2^2 \leq \|\Delta \theta\|_2 \|\theta\|_2 \quad (\text{D } 7)$$

which leads to (3.11) in which the constant $c_{5,m}$ has been re-labelled as c_m .

REFERENCES

- ANDREWS, M. J. & DALZIEL, S. B. 2010 Small Atwood number Rayleigh-Taylor experiments. *Phil. Trans. R. Soc. Ser. A* **368** (1916), 1663–79.
- CABOT, W. H. & COOK, A. W. 2006 Reynolds number effects on Rayleigh-Taylor instability with possible implications for type Ia supernovae. *Nat. Phys.* **2** (8), 562–568.
- COOK, A. W. & DIMOTAKIS, P. E. 2001 Transition stages of Rayleigh-Taylor instability between miscible fluids. *J. Fluid Mech.* **443**, 69–99.
- DAVIES-WYKES, M. S. & DALZIEL, S. B. 2014 Efficient mixing in stratified flows: experimental study of a Rayleigh-Taylor unstable interface within an otherwise stable stratification.
- DIMONTE, G., YOUNGS, D. L., DIMITS, A., WEBER, S., MARINAK, M., WUNSCH, S., GARASI, C., ROBINSON, A., ANDREWS, M. J., RAMAPRABHU, P., CALDER, A. C., FRYXELL, B., BIELLO, J., DURSI, L., MACNEICE, P., OLSON, K., RICKER, P., ROSNER, R., TIMMES, F., TUFO, H., YOUNG, Y.-N. & ZINGALE, M. 2004 A comparative study of the turbulent

- Rayleigh-Taylor instability using high-resolution three-dimensional numerical simulations: The Alpha-Group collaboration. *Phys. Fluids* **16**, 1668–1693.
- DIMOTAKIS, P. E. 2005 Turbulent mixing. *Annu. Rev. Fluid Mech.* **37**, 329–356.
- DONZIS, D.A., GIBBON, J.D., KERR, R.M., GUPTA, A., PANDIT, R. & VINCENZI, D. 2013 Vorticity moments in four numerical simulations of the 3d Navier-Stokes equations. *J. Fluid Mech.* **732**, 316–331.
- GIBBON, J.D., DONZIS, D. A., KERR, R.M., GUPTA, A., PANDIT, R. & VINCENZI, D. 2014 Regimes of nonlinear depletion and regularity in the 3d navier-stokes equations. *Nonlinearity* **27**, 1–19.
- GIBBON, J. D. 2015 High-low frequency slaving and regularity issues in the 3d Navier-Stokes equations. *IMA Journal of Applied Mathematics* pp. 1–13.
- GLIMM, J., GROVE, J. W., LI, X. L., OH, W. & SHARP, D. H. 2001 A critical analysis of Rayleigh-Taylor growth rates. *J. Comp. Phys.* **169** (2), 652–677.
- HYUNSUN, L., HYEONSEONG, J., YAN, Y. & GLIMM, J. 2008 On validation of turbulent mixing simulations for Rayleigh-Taylor instability. *Phys. Fluids* **20**, 012102–012102–8.
- LAWRIE, A. G. W. & DALZIEL, S. B. 2011 Rayleigh-Taylor mixing in an otherwise stable stratification. *J. Fluid Mech.* **688**, 507–527.
- LEE, H., JIN, H., YU, Y. & GLIMM, J. 2008 On validation of turbulent mixing simulations for Rayleigh-Taylor instability. *Phys. Fluids* **20**, 1–8.
- LIVESCU, D. 2013 Numerical simulations of two-fluid mixing at large density ratios and applications to the Rayleigh-Taylor instability. *Phil. Trans. R. Soc. A.* **371**, 20120185.
- LIVESCU, D., CANADA, C., KANOV, K., BURNS, R. & PULIDO, J. 2014 Homogeneous buoyancy driven turbulence data set. *LA-UR-14-20669* .
- LIVESCU, D., MOHD-YUSOF, J., PETERSEN, M.R. & GROVE, J.W. 2009 A computer code for direct numerical simulation of turbulent flows. *Tech. Rep.* LA-CC-09-100. Los Alamos National Laboratory.
- LIVESCU, D. & RISTORCELLI, J. R. 2007 Buoyancy-driven variable-density turbulence. *J. Fluid Mech.* **591**, 43–71.
- LIVESCU, D. & RISTORCELLI, J. R. 2008 Variable-density mixing in buoyancy-driven turbulence. *J. Fluid Mech.* **605**, 145–180.
- LUO, G. & HOU, T. 2014a Potentially singular solutions of the 3d axisymmetric euler equations. *Proc. Nat. Acad. Sci.* **111**, 12968–12973.
- LUO, G. & HOU, T. 2014b Toward the finite time blow-up of the 3d incompressible euler equations: a numerical investigation. *Multiscale model. simul.* **12**, 1722–1776.
- PETRASSO, R. D. 1994 Rayleigh’s challenge endures. *Nat. Phys.* **367** (6460), 217–218.
- RAYLEIGH, LORD 1900 Investigation of the character of the equilibrium of an incompressible heavy fluid of variable density. *Scientific Papers* **2**, 598.
- SHARP, D. H. 1984 An overview of Rayleigh-Taylor Instability. *Physica D* **12D**, 3–18.
- TAILLEUX, R. 2013 Available potential energy and exergy in stratified fluids. *Annu. Rev. Fluid Mech.* **45**, 35–58.
- TAYLOR, G. I. 1950 The instability of liquid surfaces when accelerated in a direction perpendicular to their planes. I. *Proc. R. Soc. A* **201** (1065), 192–196.
- YOUNGS, DAVID L. 1984 Numerical simulation of turbulent mixing by Rayleigh-Taylor instability. *Physica D: Nonlinear Phenomena* **12** (1-3), 32–44.
- YOUNGS, DAVID L. 1989 Modelling turbulent mixing by Rayleigh-Taylor instability. *Physica D: Nonlinear Phenomena* **37**, 270–287.